Precision Agriculture
https://doi.org/10.1007/s11119-020-09735-1

A new color index for vegetation segmentation and classification

Moon-Kyu Lee[1] · **Mahmood Reza Golzarian**[2] · **Inki Kim**[3]

Abstract
Color vegetation indices enable various precision agriculture applications by transforming a 3D-color image into its 1D-grayscale counterpart, such that the color of vegetation pixels can be accentuated, while those of nonvegetation pixels are attenuated. The quality of the transformation is essential to the outcomes of computational analyses to follow. The objective of this article is to propose a new vegetation index, the Elliptical Color Index (ECI), which leverages the quadratic discriminant analysis of 3D-color images along a normalized red (r)—green (g) plane. The proposed index is defined as an ellipse function of r and g variables with a shape parameter. For comparison, the ECI's performance was evaluated along with six other indices, by using 240 color images as a test sample captured from four vegetation species under different illumination and background conditions, together with the corresponding ground-truth patterns. For comparative analysis, the receiver operating characteristic (ROC) and the precision–recall (PR) curves helped quantify the overall performance of vegetation segmentation across all of the vegetation indices evaluated. For a practical appraisal of vegetation segmentation outcomes, this paper applied Gaussian filtering, and then the thresholding method of Otsu, to the grayscale images transformed by each of the indices. Overall, the test results confirmed that ECI outperforms the other indices, in terms of the area under the curves of ROC and PR, as well as other performance metrics, including total error, precision, and F-score.

Keywords Vegetation segmentation · Color vegetation index · Weed control · Discriminant analysis

✉ Moon-Kyu Lee
mkl3607@gmail.com

[1] Department of Industrial Engineering, Keimyung University, Daegu, Republic of Korea

[2] Department of Biosystems Engineering, Ferdowsi University of Mashhad, Mashhad, Iran

[3] Coordinated Science Lab., University of Illinois at Urbana–Champaign, Champaign, USA

Published online: 04 July 2020

Introduction

Effective weed control in precision agriculture (PA) requires the spraying of herbicides to be precisely targeted at the weed-covered spots at the right time (Wong et al. 2014). The continued increases in crop loss due to weeds and crop diseases further warrant active weed control. To that end, precise detection of weeds on agricultural fields is vital to identifying target spots for concentrated herbicides application. In contrast, a failure with precise weed detection may cause herbicides to be wasted in the field, further damaging the biophysical strength of crops and environment. Therefore, weed control has been an important issue in PA (Wobbecke et al. 1995; Burgos-Artizzu et al. 2011; Hamuda et al. 2016; Sazbi et al. 2018).

For effective PA applications, including weed control and crop/field status monitoring, computer vision is useful to process various agricultural field images. A typical image may include multiple vegetation species in a mix of crop plants and weeds, under variable background conditions. Weed detection based on computer vision requires a series of image processing operations, namely image acquisition, vegetation segmentation, feature extraction, and classification of vegetation species.

The detection of vegetation in a digital field image is the very first step to discriminate weeds from crops, and color vegetation indices (CVIs) are typically used to take advantage of the inherent color properties of green vegetation. A CVI is defined as a mathematical function of red (R), green (G), and blue (B) values in a color pallet (or their normalized values denoted by r, g, and b for each image pixel). Proposed CVIs abound in the literature; ones cited frequently include Excess Green Index (ExG) (Woebbecke et al. 1995), Excess Red Index (ExR) (Meyer and Neto 2008), Green Leaf Index (GLI) (Louhaichi et al. 2001), Hue (Cheng et al. 2001), Color Index of Vegetation Extraction (CIVE) (Kataoka et al. 2003), Modified Excess Green Index (MEGI) (Mao et al. 2003), Normalized Green–Red Difference Index (NGRDI) (Hunt et al. 2005), Vegetation Index (VEG) (Hague et al. 2006), Excess Green minus Red Index (ExGR) (Meyer and Neto 2008), and more recently, Combined Indices (COM) (Guijarro et al. 2011 (COM1); Guerrero et al. 2012 (COM2)), Modified ExG (MExG) (Burgos-Artizzu et al. 2011), Modified Green Red Vegetation Index (MGVRI) (Bendig et al. 2015), and Red Green Blue Vegetation Index (RGBVI) (Bendig et al. 2015). By applying a CVI, a color field image of RGB channels is converted to a single dimensional grayscale image, where vegetation colors are highlighted. Then, vegetation segmentation can be facilitated by classifying pixels of interests through thresholding the grayscale image, grouping equally classified pixels, and post-processing, such as morphology operations on the pixel groups. One of the well-known thresholding algorithms is the Otsu method (Otsu 1979).

A large body of research on vegetation segmentation has relied on this simple transformation, either by using a single CVI or combination of the CVIs. The CVIs frequently used in vegetation segmentation studies include CIVE (Tosaka et al. 1998), ExG (Suh et al. 2018), MEGI (Tang et al. 2003), NGRDI (Hunt et al. 2005), VEG (Hague et al. 2006), Hue (Hassanein et al. 2018), and ExGR (Neto et al. 2006; Meyer and Neto 2008). For example, Suh et al. (2018) proposed an algorithm for ground shadow detection and removal, to discriminate vegetation regions in sugar beet images taken under various illumination and weather conditions. This study used the ExG index to obtain grayscale images for thresholding.

The quality of vegetation segmentation spreads into the subsequent image processing, such as vegetation species classification, because various textural and/or shape features

to be used for classification rely on segmented vegetation objects. The high-performance requirements of PA applications have stimulated diverse approaches geared towards more accurate and faster segmentation (Hamuda et al. 2016). For example, Bai et al. (2014) proposed a segmentation technique to discriminate rice against backgrounds based on the particle swarm optimization and morphology color modeling for images that are represented in the L*a*b* color space, where L, a*, and b* stand for light intensity, the green–red color component, and the blue–yellow color component, respectively.

Many comparative studies have revealed the strength and weakness of different CVIs in segmentation performance. The CVI-based segmentation can also be used as a reference to assess the performance of other segmentation methods (Zheng et al. 2009, 2010; Yu et al. 2013; Bai et al. 2014; Guo et al. 2013; Ye et al. 2015). Table 1 summarizes the performances of the CVIs applied to the segmentation of crops like soybean, rice, and wheat from background. No single CVI guarantees best performance across different vegetation species.

Generally speaking, the classification of mixed vegetation species (e.g., weeds versus a crop) is a more intractable and complex problem, compared with segmentation from background, due to the high similarities in greenness between the vegetation colors. Only a set of classification methods sophisticated enough to handle the variation in greenness among vegetation species can be successful. To solve the classification problem, a CVI has often been utilized as a first tool to generate a grayscale image that intensifies features of green color pixels in the original RGB image. ExG has been the most popular index as a grayscale image generator (Nieuwenhuizen et al. 2010; Kazmi et al. 2015; Bah et al. 2018; Suh et al. 2018). Shape and/or textural features are then extracted from the grayscale images for the classification. Along with (or without) the shape/textural features, some CVIs themselves have been used as color features (Golzarian and Frick 2011; Kazmi et al. 2015; Milioto et al. 2018; Sazbi et al. 2018).

For the PA applications in crop status monitoring, such as nutrient contents estimation (Zheng et al. 2018), and disease spots segmentation (Ma et al. 2017), some of the CVIs have been used to produce useful features. In particular, Ma et al. (2017) proposed a comprehensive color feature combining ExR, hue, and b* component of the L*a*b* color space for segmenting foliar disease spots from cucumber downy mildew images.

The above literature review shows that diverse CVIs have been proposed and utilized in various PA areas, such as vegetation detection or segmentation, classification, disease spot segmentation, and even for crop growth/nutrition estimation. It is very clear that the CVIs used for a specific application critically affect the application performance. However, most of the vegetation indices proposed to date were intuitively or empirically developed by focusing on the difference between the green color component and the others of each pixel, without any theoretical consideration of CVI function shapes. Therefore, such indices often fail to yield robust performance and adaptability to a wide variety of image conditions.

This paper aims to propose and validate a new CVI that exploits theoretically driven physical distribution characteristics of green vegetation pixels over a normalized *rgb* color space. To challenge the problems of existing indices (i.e., those developed to serve for narrowly focused image properties or specific image instances, and which thus would yield unpredictable and unreliable performance when applied to segmentation), this paper first establishes a comprehensive performance evaluation scheme, based on which the proposed CVI together with existing ones will be tested. The following three hypotheses are set for statistical testing:

H_{0a} The new index will significantly outperform existing indices in terms of segmentation performance.

Table 1 A summary of comparative studies for evaluating the segmentation performance of different CVIs

Authors	CVIs used	Segmented vegetation species	Best CVI found
Woebbecke et al. (1995)	*r-g, g-b,* (*g-b*)/|*r-g*|, ExG, Hue	Cocklebur, velvetleaf	Hue
Meyer and Neto (2008)	ExG, ExGR, NGRDI	Soybean	ExGR
Golzarian et al. (2012)	*g*, ExG, MEGI, *g-r*, NGRDI, Hue	Wheat, ryegrass, brome grass, fodder oat	Hue
Lee and Lee (2011)	R, G, B, *r*, *g*, *b*, *g-b*, ExG, MEGI, Hue, saturation, DF = 1.2553ExG + 0.01735G-0.01474B	Rice	MEGI, DF
Zheng et al. (2009)	ExG, CIVE, SM[a]	Soybean, weeds	ExG[b]
Zheng et al. (2010)	ExGR, NGRDI, CIVE, SM[a]	Soybean, weeds	unstable performance[b]
Guijarro et al. (2011)	ExG, ExGR, CIVE, VEG, COM1	Barley, corn	COM1
Yu et al. (2013)	ExG, ExGR, CIVE, VEG, SM[a]	Maize	ExG[b]
Bai et al. (2013)	ExG, ExGR, CIVE, SM[a]	Rice	CIVE[b]
Guo et al. (2013)	ExG, MExG, ExGR, SM[a]	Wheat	ExGR[b]
Bai et al. (2014)	ExG, ExGR, SM[a]	Rice	ExG[b]
Torres-Sánchez et al. (2014)	ExG, ExGR, CIVE, (*g-b*)/(*r-g*), NGRDI, VEG, COM1, COM2	Wheat	ExG, VEG
Ye et al. (2015)	ExG, NGRDI, CIVE, VEG, SM[a]	Cotton, corn	CIVE[b]
Barbosa et al. (2019)	ExG, NGRDI, VEG, MGVRI, GLI, RGBVI	Emerald grass	NGRDI, MGVRI
Rico-Fernández et al. (2019)	ExG, CIVE, VEG, MExG, COM1, COM2	Carrot, maize, tomato	CIVE

[a]Implies a segmentation method(s) suggested by the author(s)

[b]Denotes the best CVI except the SM

H_{0b} The new index will significantly outperform existing indices in terms of its robustness to the different image properties of background and lighting.

H_{0c} The segmentation accuracy of the new index may significantly vary depending on image properties (lighting and background conditions and vegetation species type).

Tables 4, 5, and 10 summarize the results of statistical testing at the 1% significance level for H_{0a}, Table 6 for H_{0b}, and Tables 7, 8, and 9 for H_{0c}.

The performance evaluation scheme is formulated based on the following principles: A quantitative evaluation based on multiple metrics rather than focusing on a single variable is desirable, because it is likely to provide a more balanced perspective over the segmentation performance of CVI. In addition, investigating the systematic relationships among those metrics will further guide the choice of appropriate CVI. For generalization, the CVI performance needs to be tested over the realistic variability of image properties, including different types of vegetation species, background, and lighting conditions. Besides those summative performances, index-specific procedures should be carefully examined in terms of their benefits, confidence, and limitations.

Following those principles, this paper characterized segmentation performance by using the five metrics depicted in Fig. 9 (Accuracy, F-score, Precision, Type-I and -II errors), and examined their mutual relationships by using the ROC and PR Curves in Fig. 7. For possible generalization, this paper used a group of test images that substantially vary in vegetation species, background, and lighting conditions. For qualitative inspection, the effects of setting different shape parameter values and using a smaller number of input images were examined in Fig. 6 and Table 3, respectively.

Materials and method

Image data preparation

The dataset consisting of 240 images provided by Golzarian et al. (2012) was used for the comparative performance evaluation of the new vegetation index with the existing CVIs. The original dataset was created to represent varying field conditions. Images in the dataset were captured for the four classes of vegetation species (one crop: wheat, three kinds of weed: annual ryegrass, brome grass, and wild oat), the three types of backgrounds (light soil, dark soil, and crop residue), and the two types of ambient lighting (sunny and shaded). In the "Results and discussion" section of this paper, the distinct combination of the above factors is referred to as 'image groups'. These image groups span 24 ($=4\times3\times2$) different experimental cases, each with 10 image instances. Segmentation performance was evaluated by comparing each test image processed by a CVI with its corresponding ground-truth benchmark image. The benchmark (i.e., reference) images were manually created by using photo-editing software (Paint Shop Pro, Jasc Software, MN, USA), and further enhanced to eliminate noise pixels included in vegetation segments.

Performance measures of vegetation segmentation

In order to assess the vegetation segmentation quality of the CVIs, several quantitative measures have been used in the literature. Basically, the segmentation quality indicates how well the targeted vegetation regions are separated from their backgrounds. Golzarian et al. (2012) defined Type I and Type II errors as the misclassification error

of ground-truth vegetation pixels and that of ground-truth background pixels, respectively. The terminology of quality control for manufactured products can be well applied to the two-class classification of vegetation and background. The other measures used in this paper are all derived from the 2×2 confusion matrix of classification label versus true class, which consists of true positive (TP), false positive (FP), true negative (TN), and false negative (FN). TP is the number of reference vegetation pixels correctly segmented as vegetation, while FN denotes that of the remaining reference vegetation pixels misclassified as background area. Similarly, TN and FP stand for the number of reference background pixels correctly segmented as background area, and that of remaining pixels misclassified as vegetation, respectively. Then, segmentation quality measures can be calculated in terms of the following equations:

$$\text{Type I error} = \text{FN}/(\text{TP} + \text{FN}) \tag{1}$$

$$\text{Type II error} = \text{FP}/(\text{TN} + \text{FP}) \tag{2}$$

$$\text{Total error} = \text{Type I error} + \text{Type II error}$$

$$\text{Recall} = \text{Sensitivity} = \text{TP}/(\text{TP} + \text{FN}) = 1 - \text{Type I error} \tag{3}$$

$$\text{Accuracy} = (\text{TP} + \text{TN})/(\text{TP} + \text{TN} + \text{FP} + \text{FN}) \tag{4}$$

$$\text{Specificity} = \text{TN}/(\text{TN} + \text{FP}) = 1 - \text{Type II error}$$

$$\text{Precision} = \text{TP}/(\text{TP} + \text{FP}) \tag{5}$$

$$\text{F} - \text{score (Harmonic Mean)} = 2 \times \text{Precision} \times \text{Recall}/(\text{Precision} + \text{Recall}) \tag{6}$$

The above metrics summarize different aspects of segmentation quality. For example, Precision implies the correctness of extracted vegetation pixels, whereas Recall explains how well vegetation pixels are detected through the segmentation. For a full appraisal of quality, it is desirable to evaluate multiple metrics together, or a combined one, like the F-score. Segmentation Accuracy defined by Eq. (4) has often been used in the literature (Yu et al. 2013; Ahmad et al. 2018; Hassanein et al. 2018) as an integrated measure of Sensitivity and Specificity. However, simply using Accuracy only may mislead the innate performance characteristic of a CVI (Provost et al. 1998). Yet, summative metrics could miss an important aspect of quality, which graphical methods could complement. Receiver operating characteristic (ROC) and precision–recall (PR) curves are often useful to comprehensively visualize the segmentation quality when comparing two performance measures vis-à-vis (Suh et al. 2018). The area-under-the-curve (AUC) has been used to assess how each CVI performs over the whole space of either Type I or Type II errors. An AUC value of 1 implies correct classification of all image pixels. This paper used all of the above measures and the two curves to comparatively evaluate the segmentation performance for different CVIs in various ways.

Visualization of CVI behavior

Golzarian et al. (2012) presented a geometric scheme to visualize the behavior of a CVI based on the *rg* plane, where every RGB triplet of each pixel in a color image is projected onto a 2-dimensional triangular space. The *rg* plane projection is essentially a part of the normalization process, which is made as follows (Gee et al. 2008):

$$r = R_n/(R_n + G_n + B_n), g = G_n/(R_n + G_n + B_n), b = B_n/(R_n + G_n + B_n)$$

where, $R_n = R/R_{max}$, $G_n = G/G_{max}$, and $B_n = B/B_{max}$ Practical values of R_{max}, G_{max}, and B_{max} may depend on the hardware features of camera used for image acquisition, and are typically all set to 255 s for 8 bit-color intensity images. It follows that,

$$r + g + b = 1 \tag{7}$$

If both *r* and *g* values are known, *b* can always be derived from Eq. (7) as a simple linear function. Thus, a 3D *rgb* space is reduced to the corresponding 2D *rg* space, which facilitates the interpretation of CVIs' behaviors considering only a pair of *r* and *g* variables. Another advantage of this normalization is to diminish the difficulties associated with handling illuminance variability in a field image under variable ambient lights. On the *rg* space, some of the aforementioned CVIs of interest are represented as follows:

$$\text{ExG} = 2g - r - b = 3g - 1$$

$$\text{ExR} = 1.4r - g$$

$$\text{ExGR} = \text{ExG} - \text{ExR} = 4g - 1.4r - 1$$

$$\text{NGRDI} = (g - r)/(g + r)$$

$$\text{CIVE} = -0.811g + 0.441r + 0.385b + 18.78745 = -1.196g + 0.056r + 19.17245$$

$$\text{VEG} = g/r^{0.667}(1 - r - g)^{(1-0.333)}$$

$$\text{COM1} = 0.25\text{ExG} + 0.3\text{ExGR} + 0.33\text{CIVE} + 0.12\text{VEG}$$

$$= 4.25532g - 0.40152r + 5.77691 + 0.12g/r^{0.667}(1 - r - g)^{0.333}$$

$$\text{Hue} = \tan^{-1}((g - b)/(2r - g - b)) = \tan^{-1}((2g + r - 1)/(3r - 1))$$

Vegetation segmentation using the above CVIs requires setting a threshold value, *T*, to discriminate the vegetation pixels of interest from background, as follows:

$$\text{Pixel}\ (r, g) = \text{vegetation if CVI}(r, g) \leq (\text{or} \geq) T; \text{Otherwise, Pixel}\ (r, g) = \text{background} \tag{8}$$

Then, solving for *g* in the equation,

$$\text{CVI}(r, g) = T \text{ for } T_{min} \leq T \leq T_{max}$$

gives $g = f(r, T)$, a function of r and T, by which a separation of vegetation versus background is made. Hue is an exceptional CVI having two different threshold values (T_1, T_2) for the separation, such that only the pixels in-between the two are classified as vegetation. Figure 1 illustrates the behaviour of two typical CVIs, ExGR and VEG, which show that each of the CVI functions serves as a boundary curve that, as the threshold value increases, moves upward.

Figure 2 demonstrates a real-world example of vegetation segmentation using ExGR. The pixel-wise distribution of vegetation and background regions (Fig. 2d) is shown, together with the reference image (Fig. 2b) of manually extracted vegetation (wheat) from the raw image (Fig. 2a), the vegetation image segmented by a threshold value, $T = -0.228$ (Fig. 2c), and the histogram of the number of pixels against the gray level in the ExGR grayscale image normalized in the range (0, 255) (Fig. 2e). The visual analogies of Fig. 2d and e show that the separation of vegetation and background on the *rg* plane with the threshold line, ExGR $= -0.228$, is equivalent to setting the threshold value along the corresponding 1-dimensional gray level at $T = 104$ (Fig. 2e). The segmented vegetation area contains some of the background pixels, while some of the ground-truth vegetation pixels are misclassified as background, which accounts for classification errors.

A new CVI—the elliptical color index (ECI)

Most of the CVIs reviewed here define their functions without considering the property of pixel distributions. For example, ExG merely adds the two-color-component differences, $g–r$ and $g–b$, which ends up amplifying greenness (g) in vegetation objects. All linearly formulated CVIs have empirically defined functions, whereas CIVE, COM1, COM2, and MExG were established based on data analysis.

A CVI plays the role of a boundary curve separating the whole triangular region in the *rg* plane into two parts, a vegetation region and a background one, as illustrated in Fig. 3, where the random distributions of ground-truth vegetation pixels and background pixels are presented for illustration. Depending on the type of CVIs, as the threshold value changes, the separating curve may move up and down, or rotate through a single point. Pixel distributions of ground-truth vegetation and background will differ for different images. Then, the problem of interest is to find the optimal form of the curve, which is a typical classification problem with two classes.

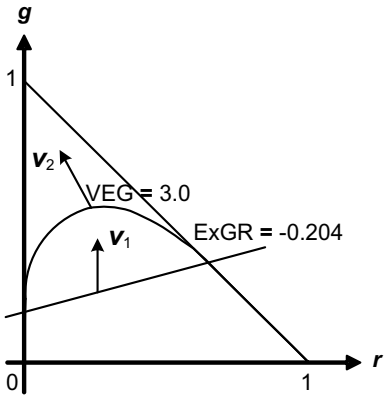

Fig. 1 Moving directions of ExGR and VEG as the threshold value increases

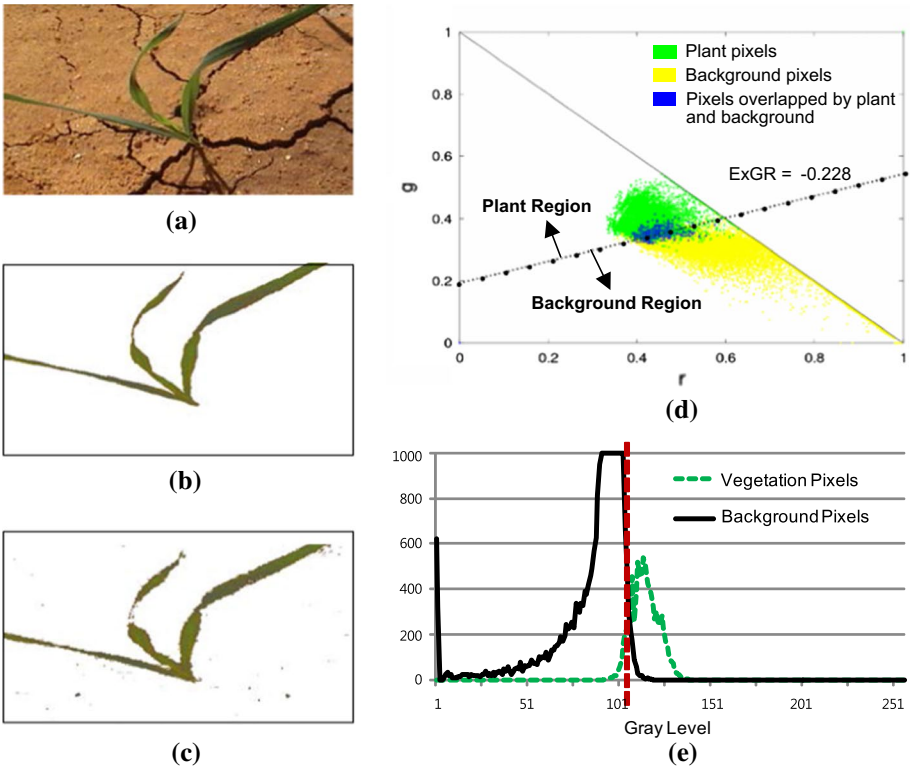

Fig. 2 An example of vegetation segmentation using ExGR: **a** An RGB image, **b** Reference image of wheat, **c** Segmented plant with $T = -0.228$, **d** Pixel distribution with the ExGR line for $T = -0.228$, **e** Histograms of vegetation and background pixels

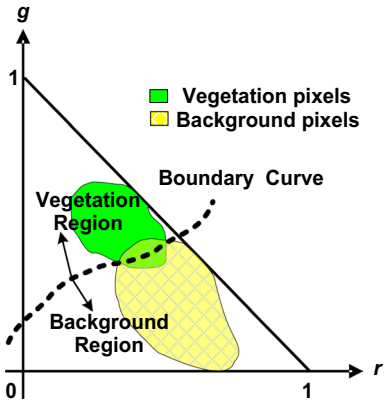

Fig. 3 A schematic of the boundary curve dividing the triangular area into vegetation and background regions

For implementation simplicity and interpretability, linear CVIs are often the first choice for practical image segmentation. If an image data reveals clear linear separability between the two classes, they can be the best empirical choice. However, image data in practice

usually shows complex data structures that are far from being linearly separated. In this regard, this paper proposes a new quadratic type of CVI based on discriminant analysis (Tharwat 2016), which is superior in discriminating such complex image data. Discriminant analysis has an advantage as a classifier over other sophisticated ones, like random decision forest and artificial neural network, in that it can provide a clear form of the mathematical boundary function, called a decision boundary, between every pair of classes. A discriminant analysis algorithm maximizes the likelihood that an item to be classified is assigned to its ground-truth class. The likelihood is represented as a posterior probability in the form of a conditional probability density function based on the Bayes rule. Let $\boldsymbol{x}$ be a random-variable vector consisting of m features defined for an individual object to be labeled as class c_i, ($i=1, \ldots, n_c$). The posterior probability that $\boldsymbol{x}$ belongs to class i will be expressed as:

$$P(c_i|x) = P(x|c_i)P(c_i)/P(x)$$

where $P(c_i)$ is the prior probability density function of c_i. Assuming the normality (i.e., a Gaussian distribution) of $P(x|c_i)$ with mean and covariance matrix being $\boldsymbol{\mu}_i$ and Σ_i, respectively, gives:

$$P(x|c_i) = \frac{1}{\sqrt{(2\pi)^{\mathrm{m}}\left|\sum_i\right|}} exp\left(-\frac{1}{2}\left(x-\mu_i\right)^T\sum_i^{-1}\left(x-\mu_i\right)\right)$$

Then, the discriminant function for class i is defined by:

$$f_i(x) = \ln P(c_i|x)$$

where ln denotes the natural logarithm. For convenience of calculation, ignoring $P(\boldsymbol{x})$ due to the independence among classes yields:

$$f_i(x) = \ln(P(x|c_i)P(c_i))$$

$$= -\frac{1}{2}\sum_i^{-1}\left(x^T\mathrm{X} + \mu_i^T\mu_i - 2\mu_i^T x\right) - \frac{\mathrm{m}}{2}\ln(2\pi) - \left(\ln\left|\sum_i\right|\right)\Big/2 + \ln\left(p\left(c_i\right)\right)$$

The decision boundary between classes i and j becomes a hyper plane separating the two classes, and is expressed as the difference between the two discriminant functions:

$$B(x) = f_i(x) - f_j(x)$$

$$-\frac{1}{2}\boldsymbol{x}^T\left(\sum_i^{-1} - \sum_j^{-1}\right)\boldsymbol{x} + \left(\boldsymbol{\mu}_i^T\sum_{\mathrm{i}}^{-1} - \boldsymbol{\mu}_j^T\sum_j^{-1}\right)\boldsymbol{x}$$
$$-\frac{1}{2}\left(\boldsymbol{\mu}_i^T\sum_i^{-1}\boldsymbol{\mu}_i - \boldsymbol{\mu}_j^T\sum_j^{-1}\boldsymbol{\mu}_j + \ln\left|\sum_i\right| - \ln\left|\sum_j\right|\right) + \ln\frac{p\left(c_i\right)}{p\left(c_j\right)}$$

$$= \boldsymbol{x}^T A_1\boldsymbol{x} + \boldsymbol{a}^T\boldsymbol{x} + A_0$$

where $\boldsymbol{A}_1 = -\frac{1}{2}\left(\sum_i^{-1} - \sum_j^{-1}\right)$, $\boldsymbol{a} = \boldsymbol{\mu}_i^T\sum_i^{-1} - \boldsymbol{\mu}_j^T\sum_j^{-1}$ and $\boldsymbol{A}_0 = -\frac{1}{2}\left(\boldsymbol{\mu}_i^T\sum_i^{-1}\boldsymbol{\mu}_i - \boldsymbol{\mu}_j^T\sum_j^{-1}\boldsymbol{\mu}_j + \ln\left|\sum_i\right| - \ln\left|\sum_j\right|\right) + \ln\frac{p(c_i)}{p(c_j)}$. If the two classes have the

same covariance matrix, i.e., $\Sigma_i = \Sigma_j$, the quadratic term disappears, and thus the decision boundary reduces to a simple linear function, like the linear CVIs. However in practical applications, this condition is rarely satisfied, since background pixels tend to be scattered to much larger areas than those of vegetation pixels, as Fig. 2d illustrates.

Now, consider a simple, two-class classification, where an individual item is characterized by two different feature measurements. The vegetation segmentation problem is an instance of this, in that there are the two classes of vegetation pixels and non-vegetation (background) ones, and each pixel is color-coded with r and g values. In this case, a decision boundary curve becomes a quadratic function of r and g with coefficients, d_k ($k = 1, \ldots, 6$):

$$B(x) = d_1 g^2 + d_2 r^2 + d_3 gr + d_4 g + d_5 r + d_6 \tag{9}$$

The covariance matrix of class i ($i = 1, 2$), is a 2×2 matrix:

$$\sum_i = \begin{pmatrix} \sigma_{i,1}^2 & \sigma_{i,12} \\ \sigma_{i,21} & \sigma_{i,2}^2 \end{pmatrix}$$

where $\sigma_{i,j}^2$ = variance of measurement j ($j = 1, 2$), for class i, and $\sigma_{i,12} = \sigma_{i,21}$ = covariance of measurements 1 and 2 for class i. The covariance of the vegetation pixels and that of the background ones for all of the 240 test images were found to be $\sigma_{1,12} = 0.00023$ and $\sigma_{2,12} = -0.00298$. Based on these small covariance values, zero covariance is assumed for both classes, which results in the diagonality of the covariance matrices. Then, the term '$d_3 gr$' in Eq. (9) can be deleted; and therefore, $B(\boldsymbol{x})$ reduces to the following elliptical form, which is more tractable and easier to predict and visualize its behavior, as follows:

$$B(x) = d_1 \left(g - g_0\right)^2 + d_2 (r - r_0)^2 + d_3 \tag{10}$$

It should be noted that d_3 in Eq. (10) will be further removed and absorbed into the threshold value, T, when the decision boundary is used for segmentation using the following equation:

$$B(x) = T$$

Consequently, the resulting $B(\boldsymbol{x})$ becomes an ellipse curve. Motivated by this elliptical form of decision boundary, this paper proposes a CVI that is defined as an ellipse with three control parameters, g_0, r_0, and d:

$$\mathrm{ECI}(r, g) = (r - r_0)^2 + \left(g - g_0\right)^2 / d^2$$

This index has an advantage over other quadratic CVIs, such as $(g–r)(g–b)$ presented by Golzarian and Frick (2011), in that only a single vegetation region can be uniquely determined for a given threshold value.

With variations in the location of the center point (r_0, g_0) and the shape parameter d, a segmented vegetation region may fluctuate with the shape of the boundary curve, which provides flexibility in classification decision. However, in this paper, (r_0, g_0) is simply set to be (1, 0), and thus ECI reduces to:

$$\mathrm{ECI}(r, g) = (r - 1)^2 + g^2 / d^2 = T \text{ for } 0 \le T \le 1 + 1/d^2 \tag{11}$$

The remaining control parameter d defines the shape of the ECI curve. As the value of d decreases, the curve becomes flat; and therefore, the center part of the curve approaches a straight line.

Besides the advantage of ECI over other quadratic CVIs, ECI also excels linear CVIs in terms of misclassification rate. Figure 4 illustrates a background-region segmentation by ECI with $d=0.16$, compared with the segmentation by using CIVE, against the ground-truth background pixel distribution obtained from a representative sample image averaging over 240 images. Since a misclassification rate (of incorrectly classifying true vegetation pixels as background) is subject to a specified threshold value, this comparison set the value identical for both CVIs, and for visual simplicity of the figure, the ground-truth vegetation regions are not shown. The figure confirms that because of the elliptical form of the ECI curve, the segmentation by ECI encloses a larger area of true background pixel distribution than the linear-type CVIs, such as CIVE (observed by the area of the distribution under the curve). This superior separating behavior of ECI may be able to lower the misclassification rate, compared with other linear CVIs.

A procedure to determine the optimal shape parameter value

Varying the shape parameter d in ECI defines different curves by which vegetation segmentation is to be performed. Suppose that Type II error has to be minimized, while meeting a specified target value of Type I error. This implies that the incorrect classification of background pixels as vegetation is minimized, while constraining Type I error to be no greater than a target value. Because the ECI curve divides the triangular region in the rg plane into two regions, as illustrated in Fig. 3, a vegetation region and a background one, the shape of the curve critically affects the segmentation performance. Therefore, careful selection of d in ECI contributes to enhancing the performance. Figure 5 shows a flow diagram of the simple procedure to determine the optimal value of d proposed in this paper. Each step of the procedure is as follows:

Step 1 For a set of images to be analyzed, classify the entire images into a set of distinct groups. The distinct features may come from such differences as illumination intensity, image background type, or vegetation species. If there exist other influential features that may also affect the segmentation quality, further breakdowns of the image groups are recommended. An appropriate hierarchy of image groups can be determined based on a specific application.

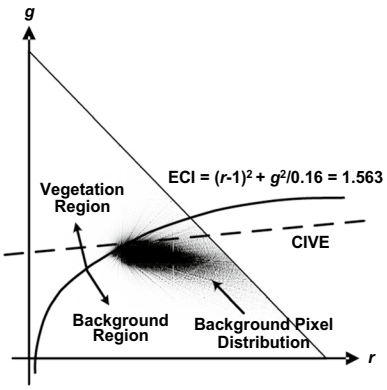

Fig. 4 An illustration of background region segmentation by using ECI and CIVE for the ground-truth background pixel distribution averaged over 240 images

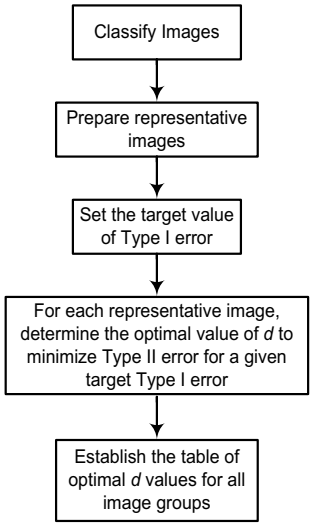

Fig. 5 A flow diagram of the procedure to determine the optimal shape parameter values for a given image set

Step 2 For each of the groups in the hierarchy, select a few prototypical images that best represent a group; and then prepare the corresponding benchmark images that mark ground-truth vegetation areas for reference. The benchmark images can be created by using a series of simple image-processing techniques. First, each of the representative images is transformed to a grayscale image by applying any one of the existing CVIs, like ExGR or ExG. Then the Otsu thresholding method is applied to the grayscale image, to discriminate the vegetation pixels from the background of the image. After this binarization, some morphology operations, such as opening and closure, are carried out to reduce noisy pixels, and to fill in empty parts of the vegetation segments, respectively. Final benchmark images will be obtained with some manual amendments, if necessary.

Step 3 Set the target value of Type I error for the segmentation performance.

Step 4 For each one of the representative images, find the optimal value of d that minimizes Type II error, while meeting the target value of Type I error. For this process, any search technique that ensures the exploration of the whole region of threshold value defined by Eq. (11) can be used.

Step 5 Establish the table of optimal d values for all of the groups. If there is more than one representative image in each group, use the average of d values found for all of the representative images included in the group.

Methods for performance comparison

Comparison using ROC and PR curves

To generate a ROC curve, for each value of Type I error (or Type II error) set in the range (0 to 1), the corresponding Type II error (or Type I error) shall be determined. Following the procedure described in the previous section, for each level of Type I error, the optimal shape parameter values were obtained for all of the 24 ($=2$ illumination types $\times 3$ background types $\times 4$ vegetation species) groups. For each group, only one representative image was chosen to estimate the shape parameter value, while the remaining 9 images were used for performance testing (note: There are 10 image instances for a distinct group, see the

"Image data preparation" section). The reason for using only a single representative image will be backed up by the experimental result described in the "Results and discussion" Section. In order to get each of the shape parameter values of the 6 (=2 illumination types×3 background types) groups, 4 parameter values found respectively from 4 vegetation species for the corresponding group were averaged.

Now, suppose that a grayscale image has been obtained by applying the ECI to a 3D color image with the parameter value found by using the shape parameter determination procedure. Then, for a given value of T, both Type I error and Type II error can be simply calculated under the classification rule expressed in Eq. (8) by using Eqs. (1) and (2), respectively. Once the ROC curve has been constructed, the corresponding AUC value can be computed by simple interpolation. In order to evaluate the vegetation segmentation quality of the proposed ECI, its AUC value was compared with those of the 7 well-known CVIs: COM1, ExGR, ExG, Hue, CIVE, NGRDI, and VEG. The PR curves were also generated by using Recall and Precision values calculated for each set value of Type I error.

Comparison for segmentation

Through the examination of the ROC and PR curves, the ECI's overall innate properties in pixel classification will be observed. In addition, the ECI performance will be investigated as compared with other CVIs when applied to vegetation segmentation using the thresholding method of Otsu. Such an index-based segmentation has long been used in a variety of PA applications in the literature (Meyer and Neto 2008; Kazmi et al. 2015; Hamuda et al. 2016; Zhang et al. 2018; Suh et al. 2018). The first step of the index-based segmentation is to convert a 3D-color image to a grayscale image by applying a CVI. The next step is to smooth the grayscale image with a 19×19 Gaussian filter, and then binarize the smoothed image using the Otsu thresholding method. The final image is obtained by applying some posterior image-processing operations, such as expanding segmented parts, and filling in apertures to the binarized image. For simplicity, in this paper, no post-processing is conducted once the binarized image is obtained.

Meyer and Neto (2008) proposed ExGR for a CVI that has a fixed, built-in zero threshold, so that no thresholding method for binarization is needed. However, using ExGR with the fixed threshold of zero had to be dropped, because it created severe under-segmentation results for most of the test images used in this paper; over 35% of Type I errors on average, which is not acceptable in most applications. Alternatively, the Otsu method was applied to the indexed grayscale images, much the same way as other CVIs. Hue index was not considered either, since it requires at least two thresholds for binarization. For each of the CVIs chosen for comparison, all of the aforementioned performance measures were computed on the binarized test images, and used to evaluate the segmentation performance.

Results and discussion

Determination of the shape parameter value

Most CVIs do not parameterize their functional form along the r and g dimensions. This fixed form of the functions is simple to use in practical applications. However, this advantage may quickly diminish with the lack of flexibility in dealing with realistic variations of the intensity of illumination, background types, vegetation species, and so on. ECI has

Table 2 The average optimal d values of the image groups for different type I errors

Image group	Type I error (%)			
	0.5	1	5	10
Sunny				
Light soil	0.40	0.38	0.40	0.44
Dark soil	0.39	0.44	0.61	0.69
Crop residue	0.38	0.38	0.48	0.56
Average	0.39	0.40	0.49	0.56
Shaded				
Light soil	0.46	0.51	0.60	0.65
Dark soil	0.50	0.56	0.72	0.79
Crop residue	0.44	0.46	0.57	0.65
Average	0.47	0.51	0.63	0.70

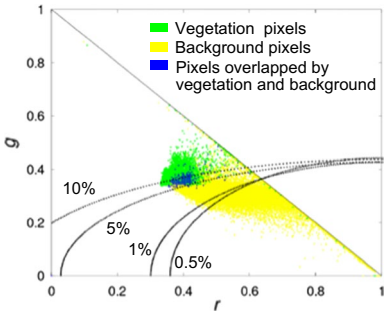

Fig. 6 ECI curves with the average optimal d values of different Type I errors for a dark-soil crop image under direct sunlight

a single parameter, d, which allows the transformation of an RGB image to be fine-tuned for a specific ambient condition into its grayscale image counterpart. The flexibility in the functional shape of ECI can potentially offer better segmentation results.

For a specified value of Type I error on a given image, the corresponding Type II error obviously depends on the value of the parameter, d, in a systematic manner. Therefore, a search to find the optimal value of d that minimizes the Type II error, while meeting the target value of Type I error, is necessary. For each specified target value of Type I error, an optimal d value of an image was empirically found by applying Step 4 of the shape parameter value determination procedure. Table 2 summarizes the optimal d value averaged over four representative images, each of which represents a vegetation species, for each of the illumination and background combination groups. Note from the table that as Type I error increases, so does the optimal d value. This trend is illustrated for a dark-soil crop image under direct sunlight in Fig. 6, where the ECI curve obtained by using the average optimal d value for each of the Type I errors of (0.5, 1, 5, and 10) % is depicted. As can be observed in the figure, as the Type I error becomes larger, a partial section of the ECI curve approaches a linear curve. This observation may support the use of linear CVIs like ExGR, ExG, CIVE, or NGRDI,

only for the cases where large Type I errors are practically allowed. Also, the optimal d values for the images taken under shade were far greater than those in sunny areas. Finally in general, the dark soil images appear to require larger values of d.

Effect of the number of representative images

A procedure was presented in the "Materials and method" section to determine the optimal shape parameter value for a given set of images. An important step in the procedure is to determine the total number of representative images for each image group. Recall that for the image dataset used in this study, there are 10 images for each combination of illumination and background type, and vegetation species. Some of the 10 images can be used to calculate the shape parameter d, and the others for performance testing. This section investigates how the segmentation performance changes according to the variation in the number of representative images in each image group. The numbers considered for the experiments were set to (1 to 5). The test images of each image group were fixed at an arbitrarily selected set of 5 images across all of the experiments.

A practically important region (PIR) of the ROC curve lies in the upper section of the curve, where the Type I error is not greater than 10%, and in turn, the sensitivity is not less than 90%. The reason for confining the practical importance to under an acceptable Type I error is that a large Type I error implies a great missing of vegetation areas from field images, which may fatally fail in a segmentation application. Note that the perfect segmentation in the overall and the reduced regions will yield the AUC values of (1 and 0.1), respectively. Table 3 summarizes the AUC values of the experimental results. From the table, no significant differences are observed in the overall segmentation performance, counter to the intuition that a larger number of representative images will yield better performance. Therefore, to minimize the computational burden and time, only a single representative image will be used for the performance evaluation of ECI.

Overall performance evaluation using the ROC and PR curves

For each of the target Type I errors, (0.1, 0.3, 0.7, 0.9, 1, 3, 5, 7, 9, 10, 30, 50, 70, and 90) %, the average Type II errors of the 216 ($=9\times24$) test images for all of the CVIs considered were calculated. The minimum average Type II error was always obtained by ECI for each of the target Type I errors. This observation is graphically verified by using the ROC curves and their enlarged upper sections (i.e., PIRs) of the eight CVIs, as shown in Fig. 7a and b. Table 4 summarizes the AUCs for the CVIs that represent overall quantitative performance. For some practically unimportant region (the region with unacceptably high Type I error), the PR curve given in Fig. 7c shows that ECI performs slightly lower in Precision than Hue and NGRDI. Overall, ECI outperformed the

Table 3 AUC values for different numbers of representative images

ROC curve	Number of representative images				
	1	2	3	4	5
Overall	0.9915	0.9912	0.9913	0.9912	0.9912
PIR	0.0949	0.0948	0.0948	0.0947	0.0947

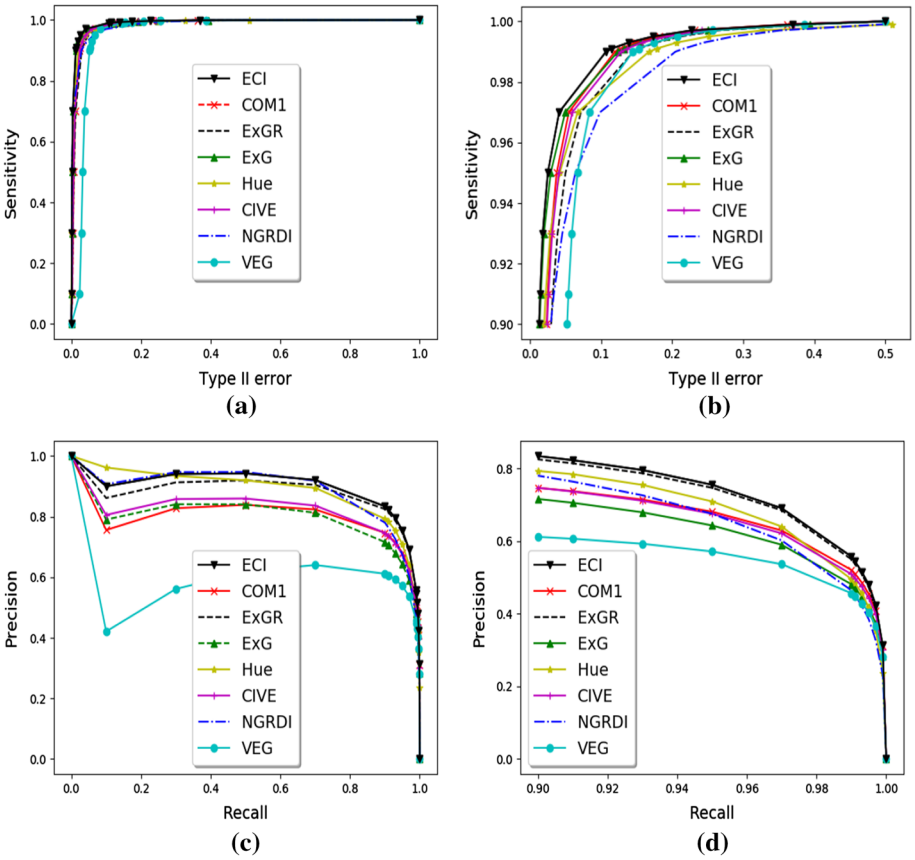

Fig. 7 ROC and PR curves: **a** ROC curve, **b** ROC curve for the PIR, **c** PR curve, and **d** PR curve for the PIR

Table 4 AUC values for the 8 CVIs

Curve	ECI	COM1	ExGR	EXG	Hue	CIVE	NGRDI	VEG
Figure 7a	0.9915	0.9858	0.9837	0.9902	0.9882	0.9862	0.9850	0.9607
Figure 7b	0.0949	0.0937	0.0923	0.0942	0.0925	0.0933	0.090	0.0909
Figure 7c	0.8055	0.7129	0.7866	0.7105	0.7918	0.7301	0.7947	0.5216
Figure 7d	0.0713	0.0647	0.0705	0.0611	0.0665	0.0641	0.0636	0.0544

other seven CVIs in the overall and PIR performances, from Table 4 and Fig. 7d. The fact that the maximum AUC values for both the ROC and PR curves were guaranteed by ECI implies its superior performance over the other CVIs. In addition, the procedure of determining the shape factor, *d*, is validated through the evaluation.

Statistical and qualitative aspects of performance

Overall comparison of color indices

A detailed evaluation of the CVIs' performance was carried out by using nonparametric statistical tests against the total errors (%) when the Type I error is fixed at 5%. The distribution of all dependent variables (i.e., CVIs) was found to be not normal according to the results from the Kolmogorov–Smirnov test, which is the same for all of the experimental results in this section. Therefore, for analysis and comparison of these variables, the non-parametric Friedman test was applied. The test results showed that the segmentation qualities of the CVIs were different at the 1% significance level ($p < 0.001$). Table 5 gives the descriptive statistics of these variables, which reveals that ECI gets first place in all of the statistics. Also, the results by the Wilcoxon signed rank test shows that there were significant differences among all pairs of color indices at the 99% confidence level, except for the two pairs, NGRDI vs. COM1 and COM1 vs. CIVE. However, the Friedman test for the three indices, NGRDI, COM1, and CIVE, shows a significant difference among them ($p < 0.001$). In particular, ExG and VEG yielded much worse performance than the other CVIs. As a result, the overall performance evaluation in terms of the total error for the color indices can be summarized as follows:

$$\text{ECI} < \text{ExGR} < \text{Hue} < \text{NGRDI} \leq \text{COM1} \leq \text{CIVE} < \text{ExG} < \text{VEG}$$

Figure 8 shows a plant image segmented by each of the 8 color indices for the raw image given in Fig. 2a, which illustrates the difference of the segmented plants and the superiority of ECI.

Image group based performance comparison

As per the hypothesis H_{0b}, the behavior of the CVIs is investigated when they are applied to the different image groups, each of which takes on distinct background, ambient lighting, and their interactions. The results of the Friedman test exhibited that there was a significant difference in the segmentation performance of the color indices. Table 6 lists mean total errors and mean ranks generated by the color indices. According to the results, ECI was found to be the best performing color index in terms of mean rank of total errors for the

Table 5 Descriptive statistics of the color indices

	Mean	Std. deviation	Minimum	Maximum	Percentiles			Mean rank
					25th	50th	75th	
ECI	7.50	3.30	5.20	35.93	5.76	6.54	7.91	2.35
COM1	8.75	4.00	5.42	41.89	6.11	7.46	9.90	4.75
ExGR	7.91	4.59	5.30	38.19	5.82	6.54	7.95	2.66
ExG	10.01	6.03	5.52	56.44	6.25	7.75	11.81	6.74
Hue	9.26	9.10	4.66	92.94	5.90	6.64	9.97	3.62
CIVE	9.06	4.80	5.45	49.39	6.12	7.27	10.33	5.21
NGRDI	11.39	12.32	5.21	95.67	5.76	6.77	11.55	4.02
VEG	11.70	6.04	5.38	41.26	6.70	9.95	15.09	6.65

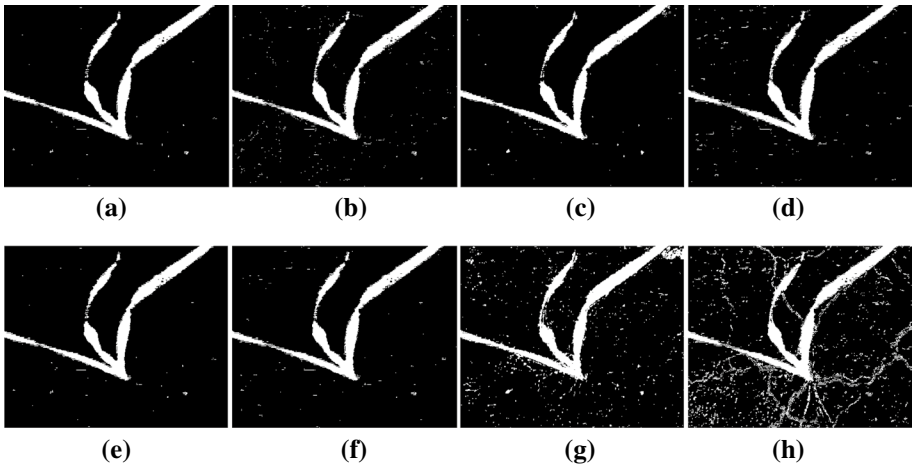

Fig. 8 Plant images segmented by using the color indices: **a** ECI, **b** COM1, **c** ExGR, **d** ExG, **e** Hue, **f** CIVE, **g** NGRDI, and **h** VEG

cases of 'sunny', 'shaded', 'light soil', 'dark soil', 'sunny light soil', 'sunny dark soil', and 'shaded crop residue'. Note that the best values are highlighted in bold for each case in the table. On the other hand, the second-best performance was achieved by ECI in some image groups of 'crop residue', 'sunny crop residue', 'shaded light soil', and 'shaded dark soil'. However, total errors of ECI and the best performing index, ExGR, for the image groups of 'crop residue', 'sunny crop residue', and 'shaded light soil', turned out to be indifferent at the 5% level of significance. It follows that ECI was shown to work best, or at least competitively with the best, for all of the 11 cases, except the 'shaded dark soil' image group, where the best performance was shown by NGRDI.

Effect of lighting condition on ECI

In the following, the effects of three qualitative factors of lighting condition, background type, and vegetation species on the segmentation quality of ECI were examined. First of all, the non-parametric Mann–Whitney test was performed to find the effect of lighting condition on ECI, and Table 7 gives the test results of this test. As can be seen, the lighting condition has a significant effect on ECI ($p < 0.001$), and ECI works better with lower total error when the images of vegetation are taken in shaded areas.

Effect of background status on ECI

Table 8 shows the effect of background condition on the segmentation performance of ECI that was examined using the non-parametric Kruskal–Wallis test. The background type affected the way ECI works ($p < 0.001$). ECI performed best for images taken from the dark soil background, where the contrast of background with vegetation color is the greatest. The largest amount of total error occurred when a complex background of crop residue was present in images. The results of the Mann–Whitney test showed that there were significant differences between each pair of background conditions ($p < 0.001$), which means that all of these conditions affect the ECI performance differently and independently.

Table 6 Mean total error (%) and mean rank (the lower, the better) for different background and lighting conditions

Case	ECI	COM1	ExGR	ExG	Hue	CIVE	NGRDI	VEG
Sunny	**8.46/2.45**	10.02/4.76	9.23/2.68	11.65/6.24	10.47/3.03	10.3/4.55	15.44/5.05	15.33/7.25
Shaded	**6.55/2.25**	7.49/4.74	6.59/2.65	8.36/7.23	8.04/4.21	7.81/5.88	7.35/2.99	8.07/6.05
Light soil	**7.25/2.71**	7.99/4.72	8.43/3.03	9.12/6.15	9.56/3.1	8.25/4.61	13.21/4.67	11.93/7.01
Dark soil	**6.17/2.47**	6.56/5.19	**6.17**/3.12	6.81/7.21	6.3/3.08	6.61/5.96	6.28/2.51	8.46/6.46
Crop residue	**9.09**/1.88	11.71/4.33	9.15/**1.85**	14.09/6.85	11.9/4.68	12.32/5.07	14.7/4.88	14.71/6.47
Sunny light soil	**8.61/2.5**	9.92/4.94	10.98/3.39	11.97/5.64	13.16/2.64	10.38/3.94	20.46/5.92	16.82/7.03
Sunny dark soil	6.44/**2.61**	6.86/5	6.33/2.94	7.17/6.75	**6.24**/2.75	6.88/5.25	6.68/3.19	10.62/7.5
Sunny crop residue	**10.32**/2.25	13.28/4.33	10.4/**1.69**	15.8/6.33	12.02/3.69	13.65/4.44	19.16/6.03	18.56/7.22
Shaded light soil	5.9/2.92	6.07/4.5	**5.87/2.67**	6.28/6.67	5.96/3.56	6.12/5.28	5.95/3.42	7.05/7
Shaded dark soil	5.89/2.33	6.26/5.39	6.02/3.29	6.45/7.67	6.37/3.4	6.34/6.67	**5.87/1.83**	6.3/5.42
Shaded crop residue	**7.86/1.5**	10.14/4.33	7.89/2	12.37/7.36	11.79/5.67	10.98/5.69	10.23/3.72	10.85/5.72

a/b implies mean total error/mean rank

Each of the bold numbers implies the minimum one in each row

Table 7 Mann–Whitney test results for examining the effect of lighting condition on the total error (%) of ECI

Lighting condition	Mean	Lower quartile	Median	Upper quartile	Mean rank
Sunny	8.46	6.06	7.16	9.34	131.77
Shaded	6.55	5.65	5.97	7.05	85.23

Table 8 Kruskal–Wallis test results for assessing the effect of background conditions on the total error (%) of ECI

Background condition	Mean	Lower quartile	Median	Upper quartile	Mean rank
Light soil	7.25	5.70	6.30	7.36	97.44
Dark soil	6.17	5.60	5.79	6.46	67.38
Crop residue	9.09	7.09	7.93	9.67	160.68

Table 9 Kruskal–Wallis test results for assessing the effect of vegetation species on the total error (%) of ECI

Vegetation species	Mean	Lower quartile	Median	Upper quartile	Mean rank
Wheat	6.634	5.622	6.489	7.168	91.41
Ryegrass	8.041	6.014	7.335	9.421	132.80
Bromegrass	8.216	5.680	6.297	8.254	100.87
Wild oat	7.124	5.812	6.519	7.538	108.93

The effect of vegetation species on ECI

The results of the non-parametric Kruskal–Wallis test given in Table 9 reveal that the vegetation species affected the performance of ECI differently at the 5% significance level ($p = 0.018$). This color index was able to classify wheat with higher performance (i.e., smaller total error) than other vegetation species. The non-parametric Mann–Whitney test was used to compare each pair of vegetation species. The results indicate that there was a significant difference only between wheat and ryegrass ($p = 0.001$).

Evaluation for segmentation applications

In this section, following the methods for performance comparison described in the "Materials and method" section, the performance of the color indices was investigated in actual segmentation applications by using the method of Otsu with Gaussian filtering. Figure 9 displays the overall performance of the 7 CVIs for segmentation. Recall that for the case of perfect segmentation, the Accuracy, F-score, and Precision are all 1, whereas Type I and Type II errors are 0. Type I and Type II errors are performance indicators that independently reflect classification errors. Type I error in this paper is defined as a portion of vegetation pixels wrongly classified as background, whereas Type II error is that of background pixels misclassified as vegetation. Therefore to get acceptable segmentation results, both errors need to be minimized simultaneously. It should be noted that unlike the experiments

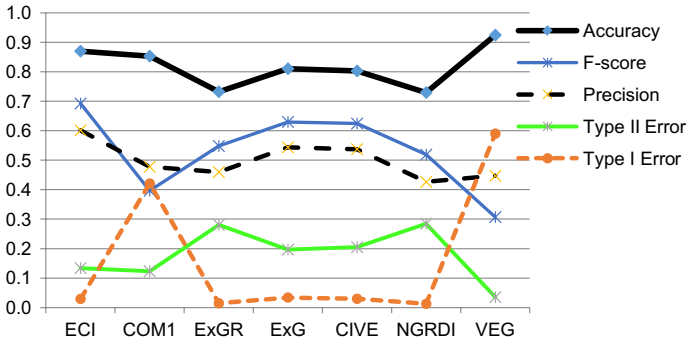

Fig. 9 Performance comparison for vegetation segmentation

Table 10 Total errors of the CVIs

	ECI	COM1	ExGR	ExG	CIVE	NGRDI	VEG
Average	0.1630	0.5442	0.2952	0.2306	0.2345	0.2974	0.6253
SD	0.2149	0.4266	0.3027	0.2663	0.2735	0.2765	0.4270

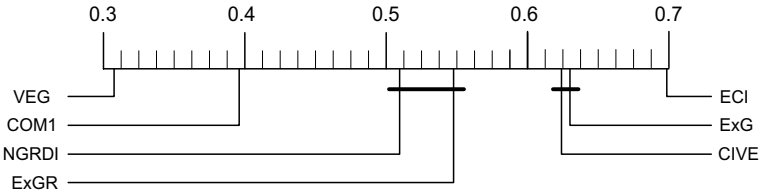

Fig. 10 F-score distributions of the 7 CVIs

for generating the ROC and PR Curves where each Type I value is fixed, and then its associated Type II error is determined, here both Type I error and Type II error for an image are simultaneously and uniquely set, when the image is segmented by the Otsu method. A significant difference in total errors of the CVIs was found at the 1% level of significance by using the Friedman test. Table 10 lists the average and standard deviation (SD) of total classification errors for each of the CVIs. ECI has the lowest total error and the standard deviation as well, which demonstrates the best classification quality among the CVIs considered in this paper.

Accuracy in Eq. (4) represents the ratio of correctly classified pixels to the total number of pixels in an image. Such accuracy measurements often bring about misleading results in the performance of VEG, as shown in Fig. 10. Although VEG has the largest accuracy value, other performance indices, such as F-score, precision, and Type I error, are worst or near worst. In such cases, high accuracy is definitely meaningless. This contradiction mainly comes from the large skewness in the pixel class distribution. Actually, the total number of vegetation pixels in many test images is much smaller than that of background pixels. Therefore, sacrificing Recall (=1- Type I error) quality excessively so as to confine Type II error to a sufficiently low value can lead to a biased, high accuracy. Consequently,

care should be taken to use the performance measure in comparative evaluations. Nevertheless, it is noteworthy that except for VEG, the largest average accuracy value was generated from ECI, and its distribution of the accuracy values was different from that of the third ranked index, COM1.

F-score, defined as the weighted harmonic mean of Precision and Recall in Eq. (6), is a good alternative to Accuracy, which may overcome the difficulties of skewed class distributions, and thereby can evaluate the overall performance well in an integrated way. ECI has the largest F-score and Precision averaged for the dataset. For both performance indicators, there were statistically significant differences between ECI and the second-best color index, ExG, at the 1% level of significance. A similar observation was made for Precision, which represents the correctness of extracted vegetation pixels in Eq. (5). Figure 10 visualizes the results of the Wilcoxon signed rank test that examines differences among the F-score distributions produced by the 7 CVIs. In the figure, statistically indifferent CVIs are connected by a bold black bar. The F-score distribution of ECI is significantly different from those of the other CVIs at the 1% significance level. On the other hand, the second-best couple, ExG and CIVE, turns out to have the same distribution. The same is true for the couple, ExGR and NGRDI. Finally, in terms of the F-score, VEG and COM1 yielded the worst performance.

It follows from the above analysis that for actual vegetation segmentation, the proposed index, ECI, was proven to outperform the other CVIs considered in this study, in terms of all of the important performance measures, F-score, Precision, and total error. Furthermore, ECI yielded the highest accuracy among the CVIs excluding VEG. Actually, the outstanding high accuracy results of VEG were made from excessive misclassification of vegetation pixels as background. Therefore, considering all of the above quantitative analyses, it is concluded that ECI is a compelling option for a grayscale image generator in vegetation segmentation.

Conclusions

Most of the existing CVI functions are formed intuitively, such that the greenness property of vegetation species is overemphasized, without reference to the mathematical logic behind vegetation segmentation. On the other hand, the proposed CVI function, ECI, is established in a mathematically logical fashion based on the discriminant analysis. The function of ECI is represented as an ellipse equation with a shape parameter in the *rg* plane. In order to estimate the parameter, only a single representative image was used for each image group. The innate segmentation quality of the 8 CVIs was investigated initially by using the ROC and PR curves. The AUC values of the curves produced from the 216 real images demonstrated that the proposed color index outperforms the other 7 CVIs. Moreover, a detailed evaluation of the CVIs for different combinations of the image conditions reveals that under most combinations of lighting condition and background type, the ECI performance excels compared with those of the other CVIs. For validation of the proposed index in practical applications, segmentation quality measures for each of the seven CVIs excluding the Hue index were collected by applying the method of Otsu with Gaussian filtering to each test image. The results show the superiority of ECI in most performance measures, including total error, Precision, and F-score. It is believed from these promising results that ECI could be used to handle more delicate vegetation segmentation problems, together with advanced classification methods like encoder–decoder convolutional neural

networks (Bah et al. 2018; Bosilj et al. 2019) for a high-performance grayscale image generator that effectively highlights the greenness features of vegetation.

Whenever a new image set is tested, an effective shape parameter value needs to be determined such that segmentation quality is maximized. The requirement of this tuning process will be a drawback of ECI for actual applications. On the other hand, this disadvantage can be interpreted as an advantage, in that it provides adaptability to various image environments, such as different luminance intensity and background status, by appropriately varying the value of the shape parameter, *d*.

References

Ahmad, J., Muhammad, K., Ahmad, I., Ahmad, W., Smith, M. L., Smith, L. N., et al. (2018). Visual features based boosted classification of weeds for real-time selective herbicide sprayer systems. *Computers in Industry, 98*, 23–33.

Bah, M. D., Hafiane, A., & Canals, R. (2018). Deep learning with unsupervised data labeling for weeds detection on UAV images. *arXiv preprint, arXiv*, 1805.12395.

Bai, X. D., Cao, Z. G., Wang, Y., Yu, Z. H., Zhang, X. F., & Li, C. N. (2013). Crop segmentation from images by morphology modeling in the CIE L*a*b* color space. *Computers and Electronics in Agriculture, 99,* 21–34.

Bai, X., Cao, Z., Wang, Y., Yu, Z., Hu, Z., Zhang, X., et al. (2014). Vegetation segmentation robust to illumination variations based on clustering and morphology modeling. *Biosystems Engineering, 125*(September), 80–97. https://doi.org/10.1016/j.biosystemseng.

Barbosa, B. D. S., Ferraz, G. A. S., Gonçalves, L. M., Marin, D. B., Maciel, D. T., Ferraz, P. F. P., et al. (2019). RGB vegetation indices applied to grass monitoring: A qualitative analysis. *Agronomy Research, 17*(2), 349–357.

Bendig, J., Yu, K., Aasen, H., Bolten, A., Bennertz, S., Broscheit, J., et al. (2015). Combining UAV-based plant height from crop surface models, visible, and near infrared vegetation indices for biomass monitoring in barley. *International Journal of Applied Earth Observation and Geoinformation, 39*, 79–87.

Bosilj, P., Aptoula, E., Duckett, T., & Cielniak, G. (2019). Transfer learning between crop types for semantic segmentation of crops versus weeds in precision agriculture. *Journal of Field Robotics*. https://doi.org/10.1002/rob.21869.

Burgos-Artizzu, X. P., Ribeiro, A., Guijarro, M., & Pajares, G. (2011). Real-time image processing for crop/weed discrimination in maize fields. *Computers and Electronics in Agriculture, 75*(2), 337–346.

Cheng, X. H., Sun, Y., & Wang, J. (2001). Color image segmentation: advances and prospects. *Pattern Recognition, 34*, 2259–2281.

Gee, Ch, Bossu, J., Jones, G., & Truchetet, F. (2008). Crop/weed discrimination in perspective agronomic images. *Computers and Electronics in Agriculture, 60*, 49–59.

Golzarian, M. R., & Frick, R. A. (2011). Classification of images of wheat, ryegrass and brome grass species at early growth stages using principal component analysis. *Plant Methods, 7*, 28–38. https://doi.org/10.1186/1746-4811-7-28.

Golzarian, M. R., Lee, M.-K., & Desbiolles, J. M. A. (2012). Evaluation of color indices for improved segmentation of plant images. *Transactions of the ASABE, 55*(1), 261–273.

Guerrero, J. M., Pajares, G., Montalvo, M., Romeo, J., & Guijarro, M. (2012). Support vector machines for crop/weeds Identification in maize fields. *Expert Systems with Applications, 39*, 11149–11155.

Guijarro, M., Pajares, G., Riomoros, I., Herrera, P. J., Burgos-Artizzu, X. P., & Ribeiro, A. (2011). Automatic segmentation of relevant textures in agricultural images. *Computers and Electronics in Agriculture, 75*(1), 75–83.

Guo, W., Rage, U. K., & Ninomiya, S. (2013). Illumination invariant segmentation of vegetation for time series wheat images based on decision tree model. *Computers and Electronics in Agriculture, 96*, 58–66.

Hague, T., Tillet, N., & Wheeler, H. (2006). Automated crop and weed monitoring in widely spaced cereals. *Precision Agriculture, 7*(1), 21–32.

Hamuda, E., Glavin, M., & Jones, E. (2016). A survey of image processing techniques for plant extraction and segmentation in the field. *Computers and Electronics in Agriculture, 125*, 184–199.

Hassanein, M., Lari, Z., & El-Sheimy, N. (2018). A new vegetation segmentation approach for cropped fields based on threshold detection from hue histogram. *Sensors, 18*(4), 1253. https://doi.org/10.3390/s18041253.

Hunt, E. R., Cavigelli, M., Daughtry, C. S. T., McMurtrey, J. E., & Walthall, C. L. (2005). Evaluation of digital photography from model aircraft for remote sensing of crop biomass and nitrogen status. *Precision Agriculture, 6*, 359–378.

Kataoka, T., Kaneko, T., Okamoto, H., & Hata, S. (2003). Crop growth estimation system using machine vision. In *Proceedings 2003 IEEE/ASME International Conference on Advanced Intelligent Mechatronics* (pp 1079–1083).

Kazmi, W., Garcia-Ruizb, F., Nielsenb, J., Rasmussen, J., & Andersen, H. (2015). Detecting creeping thistle in sugar beet fields using vegetation indices. *Computers and Electronics in Agriculture, 112*, 10–19.

Lee, K.-J., & Lee, B.-W. (2011). Estimating canopy cover from color digital camera image of rice field. *Journal of Crop Science and Biotechnology, 14*(2), 151–155.

Louhaichi, M., Borman, M. M., & Johnson, D. E. (2001). Spatially located platform and aerial photography for documentation of grazing impacts on wheat. *Geocarto International, 16*, 65–70.

Ma, J., Du, K., Zhang, L., Zheng, F., Chu, J., & Sun, Z. (2017). A segmentation method for greenhouse vegetable foliar disease spots images using color information and region growing. *Computers and Electronics in Agriculture, 142*, 110–117.

Mao, W., Wang, Y., & Wang, Y. (2003). Real-time detection of between-row weeds using machine vision. In *ASAE* Paper No. 031004, Las Vegas, Nev., USA.

Meyer, G. E., & Neto, J. C. (2008). Verification of color vegetation indices for automated crop imaging applications. *Computers and Electronics in Agriculture, 63*, 282–293.

Milioto, A., Lottes, P., & Stachniss, C. (2018). Real-time semantic segmentation of crop and weed for precision agriculture robots leveraging background knowledge in CNNs. In *Proceedings of IEEE Internationall Conference on Robotics and Automation* (ICRA) (pp. 2229–2235). Brisbane, Australia.

Neto, J. C., Meyer, G. E., & Jones, D. D. (2006). Individual leaf extractions from young canopy images using Gustafson-Kessel clustering and a genetic algorithm. *Computers and Electronics in Agriculture, 51*, 66–85.

Nieuwenhuizen, A. T., Hofstee, J. W., & van Henten, E. J. (2010). Adaptive detection of volunteer potato plants in sugar beet fields. *Precision Agriculture, 11*, 433–447.

Otsu, N. (1979). A threshold selection method from gray-level histogram. *IEEE Transactions on Systems, Man, and Cybernetics, 9*(1), 62–66.

Provost, F., Fawcett, T., & Kohavi, R. (1998). The case against accuracy estimation for comparing induction algorithms. In *Proceedings of the 15th International Conference on Machine Learning* (San Francisco, USA) (pp. 445–453).

Rico-Fernández, M. P., Rios-Cabrera, R., Castelán, M., Guerrero-Reyes, H.-I., & Juarez-Maldonado, A. (2019). A contextualized approach for segmentation of foliage in different crop species. *Computers and Electronics in Agriculture, 156*, 378–386.

Sazbi, S., Abbaspour-Gilandeh, Y., & Garcia-Mateos, G. (2018). A fast and accurate expert system for weed identification in potato crops using metaheuristic algorithms. *Computers in Industry, 98*, 80–89.

Suh, H. K., Hofstee, J. W., & van Henten, E. J. (2018). Improved vegetation segmentation with ground shadow removal using an HDR camera. *Precision Agriculture, 19*, 218–237.

Tang, L., Tian, L., & Steward, B. L. (2003). Classification of broadleaf and grass weeds using Gabor wavelets and an artificial neural network. *Transactions of the ASAE, 46*(4), 1247–1254.

Tharwat, A. (2016). Linear vs quadratic discriminant analysis classifier: A tutorial. *International Journal of Applied Pattern Recognition, 3*(2), 145–180.

Torres-Sánchez, J., Peña, J. M., de Castro, A. I., & López-Granados, F. (2014). Multitemporal mapping of the vegetation fraction in early-season wheat fields using images from UAV. *Computers and Electronics in Agriculture, 103*, 104–113. https://doi.org/10.1016/j.compag.2014.02.009.

Tosaka, N., Hata, S., Okamoto, H., & Takai, M. (1998). Automatic thinning mechanism of sugar beets (part 2). *Journal of JSAM, 60*(2), 75–82.

Woebbecke, D., Meyer, K., & Mortensen, D. (1995). Color indices for weed identification under various soil, residue and lighting conditions. *Transactions of the ASAE, 38*, 259–269.

Wong, W. K., Chekima, A., Mariappan, M., Wee, C. C., Khoo, B., & Nadarajan, M. (2014). Genetic Algorithm optimization and feature selection for a support vector machine weed recognition system in Malaysia at critical stage of development. *World Applied Sciences Journal, 30*, 1953–1959.

Ye, M., Cao, Z., Yu, Z., & Bai, X. (2015). Crop feature extraction from images with probabilistic superpixel Markov random field. *Computers and Electronics in Agriculture, 114*(June), 247–260. https://doi.org/10.1016/j.compag.2015.04.010.

Yu, Z., Cao, Z., Wu, X., Bai, X., Qin, Y., Zhuo, W., et al. (2013). Automatic image-based detection technology for two critical growth stages of maize: Emergence and three-leaf stage. *Agricultural and Forest Meteorology, 174–175*, 65–84.

Zhang, X., Li, X., Zhang, B., Zhou, J., Tian, G., Xiong, Y., et al. (2018). Automated robust crop-row detection in maize fields based on position clustering algorithm and shortest path method. *Computers and Electronics in Agriculture, 154*, 165–175.

Zheng, H., Cheng, T., Li, D., Zhou, X., Yao, X., Tian, Y., et al. (2018). Evaluation of RGB, color-infrared and multispectral images acquired from unmanned aerial systems for the estimation of nitrogen accumulation in rice. *Remote Sensing, 10*, 824. https://doi.org/10.3390/rs10060824.

Zheng, L., Shi, D., & Zhang, J. (2010). Segmentation of green vegetation of crop canopy images based on mean shift and Fisher linear discriminant. *Pattern Recognition, 31*, 920–925.

Zheng, L., Zhang, J., & Wang, Q. (2009). Mean-shift-based color segmentation of images containing green vegetation. *Computers and Electronics in Agriculture, 65*, 93–98.